

## EFFECT OF ROLLING TEXTURE ON BEARING CAPACITY OF AIRCRAFT REPAIR PATCHES AND REPLACED PANELS

Mykhailo KARUSKEVYCH  , Sergiy IGNATOVYCH , Tetiana MASLAK , Oleg KARUSKEVYCH 

*Department of Aircraft Design, National Aviation University, Kyiv, Ukraine*

### Article History:

- received 13 August 2024
- accepted 12 November 2024

**Abstract.** The article combines issues related to biaxial fatigue loading, corrections for equivalent stress calculations, and the practical application of new knowledge regarding biaxial fatigue in the aviation industry. It considers the possibility and expediency of taking into account the anisotropy of metals' mechanical characteristics in aircraft repair procedures, such as patching and replacing damaged skin panels. The biaxial loading of the skin is shown to be a significant factor that should be considered in the aircraft skin repair process. It is shown that while well-known Huber-Mises formula works well for isotropic materials, the fuselage skin made of anisotropic alloys requires corrections to the Huber-Mises method. For aircraft parts subjected to biaxial loading, the assessment of equivalent uniaxial stresses can be done by introducing the crystallographic factor into the Huber-Mises formula. This is achieved by transforming the biaxial stress components of fuselage loading due to pressurization and bending into the resolved stresses in the activated crystallographic slip systems of the dominant texture.

**Keywords:** aircraft fuselage, skin damage, biaxial loading, repair, anisotropy, texture, resolved shear stress, equivalent stress.

 Corresponding author. E-mail: [mkaruskevich@hotmail.com](mailto:mkaruskevich@hotmail.com)

## 1. Introduction

The fuselage of contemporary planes is a thin-walled semi-monocoque structure, consisting of stressed skin, supported by stringers, frames, crack stoppers, doubles, etc. Fatigue cracks, corrosion, shooting, lightning strikes and accidental mechanical damages are often critical in terms of the components' bearing capacity and fatigue life. Repair of damaged structural elements can be conducted by installation patches or replacing the skin panels. Repair parts are made from the same material as the original damaged skin.

Metal sheets used for the skin are produced by rolling. Due to plastic deformation during the rolling process, metal sheets develop a texture that defines the anisotropy of their mechanical properties. Nowadays, the anisotropy of the patch's material is not considered in fuselage repair processes, but it can have a favorable effect on the bearing capacity of the skin components.

The appearance of fatigue crack initiates repair procedures and identifies areas that require strengthening due to their susceptibility to fatigue. Enhancing the structure's resistance to fatigue can be achieved by optimizing the orientation of the patch texture.

Stress-strain analysis of aircraft structural elements working under biaxial loading conditions is currently performed using the Huber-Mises method. It is shown that the Huber-Mises formula was initially proposed for isotropic materials, whereas the fuselage skin is made of anisotropic alloys. The biaxial loading of the skin and anisotropy of patches made of rolled sheets of aluminium alloys are not considered in contemporary aircraft skin procedures, such as patching or replacing damaged skin panels. The article considers the possibility and expediency of accounting for these factors for enhance the bearing capacity of repaired aircraft parts.

This scientific problem of increasing the bearing capacity of patches and panels in a repaired fuselage is addressed in the paper by considering the following factors: a) accounting for the rolling crystallographic texture; b) calculating the resolved shear stresses in grains with dominant crystallographic orientations; c) introducing the resolved crystallographic stresses into the Huber-Mises formula; d) orienting the patch so that the corrected Huber-Mises equivalent stresses are minimized.

The aim of the research presented in the article is to develop recommendations for improving the repair procedure based on a new method for calculation equivalent stresses for materials with texture, such as those with crystallographic anisotropy caused by rolling.

## 2. Aircraft skin damage and repair

During their long service lives, aircraft structures sustain damages of different nature, levels of danger and methods for repair. The most typical include: fatigue cracks (Kuznetsov et al., 2007), corrosion (Aeronautics guide, 2023), punctures (Aviation, 2015), dents (Lafiosca et al., 2023), lightning strike damage (Dauntless aviation, 2009), bullet holes (Pikryl, 1992) (Figure 1). All these defects impact aircraft structural integrity.

Repairing the skin involves a multi-step procedure. The process begins with an analysis of the recommendations in the structural repair manual (SRM) issued by the manufacturer. For damages beyond the allowable level, the manufacturer makes the decision. The repair itself starts with cutting out the damaged area. In the case of fatigue cracks, the area in front of the crack tip must be removed.

Repair by patches can be conducted using two methods: a) lap or scab patches; b) flush patches (Federal Avia-

tion Administration [FAA], 2023). In the simplest form, the edges of the patch and the skin overlap each other and are riveted together (Figure 2a). This type of patch negatively affects the aerodynamic friction drag component for high-speed aircraft. A flush patch installation (Figure 2b) is a more complicated procedure, but it provides better aerodynamics (lower friction drag) for the outer skin. In some cases, usually due to corrosion in the fuselage bilge area, entire panels of the skin must be replaced (F1360 Aero, 2020) (Figure 2c). Details of the procedure are determined by the aircraft manufacturer.

These actions must ensure that the repair meets or exceeds the static strength and fatigue life of the original structure.

In the case of repair by replacing damaged metal, the enhancement of bearing capacity can be achieved through the intrinsic strength potential determined by texture anisotropy.

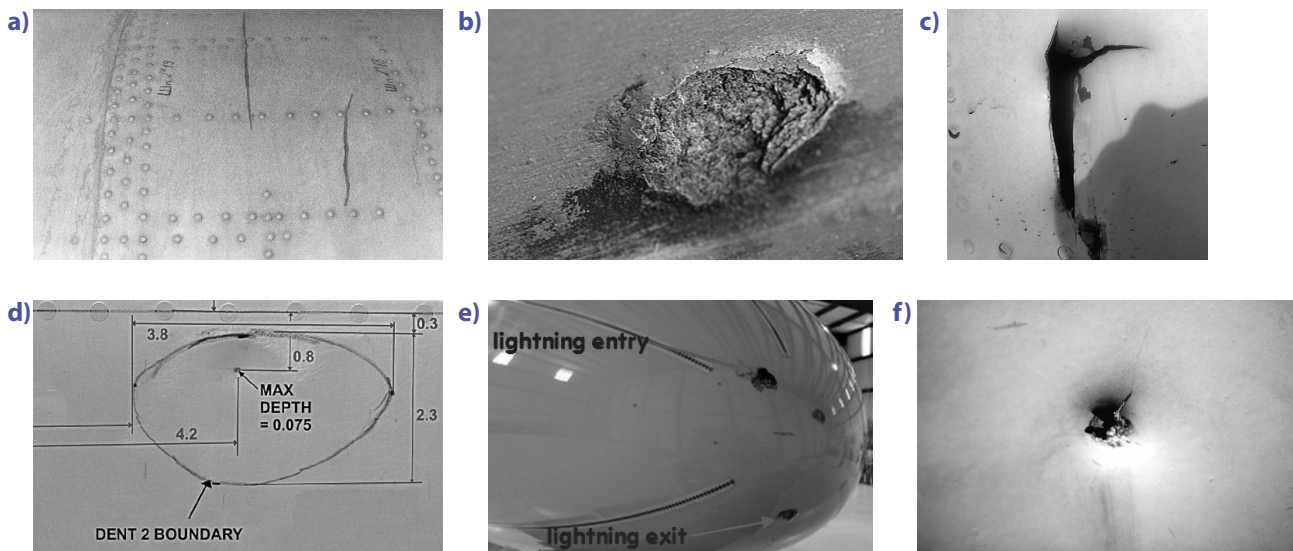


**Figure 1.** Typical operational damages of aircraft fuselage skin: a – fatigue cracks in the skin (Kuznetsov et al., 2007); b – exfoliation corrosion (Aeronautics guide, 2023); c – fuselage skin puncture (Aviation, 2015); d – skin dent (Lafiosca et al., 2023); e – lightning strike (Dauntless aviation, 2009); f – bullet hole (Pikryl, 1992)

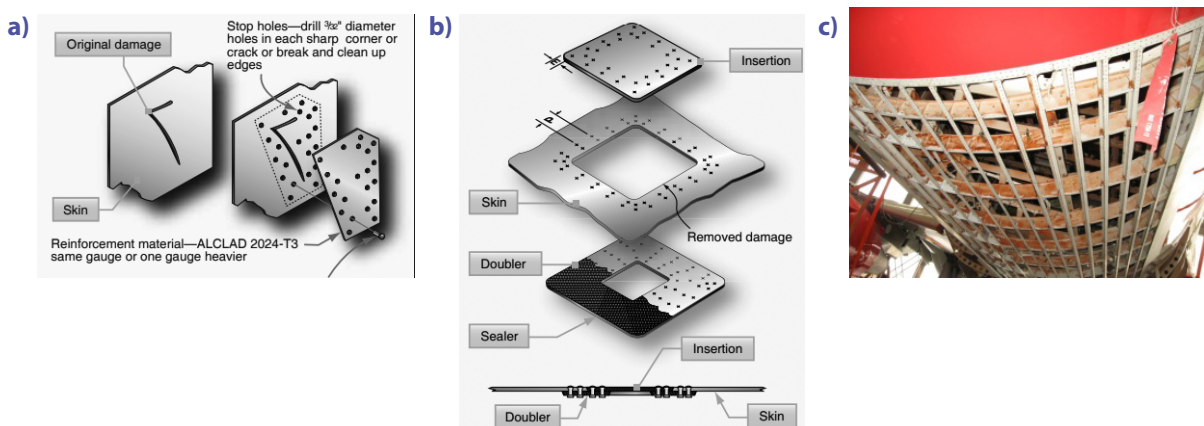


**Figure 2.** Repair procedures: a – lap patch; b – Flush patch (FAA, 2023); c – A320 belly skin panel replacement (F1360 Aero, 2020)

**Table 1.** Composition (%) of aluminium alloy 2024-T3 (source: ASM, n.d.)

Cr	Cu	Fe	Mg	Mn	Si	Ti	Zn	Al
Max 0.1	3.8–4.9	Max 0.5	1.2–1.8	0.3–0.9	Max 0.5	Max 0.15	Max 0.25	90.7–94.7

**Table 2.** Mechanical properties of 2024T3 alloy (source: ASM, n.d.)

Ultimate Tensile Strength, MPa	Yield Strength, MPa	Elongation, %
483	345	18

**Table 3.** Composition (%) of aluminium alloy 2524-T3 (source: JIMA Aluminum, n.d.)

Cu	Mg	Mn	Fe	Si	Zn	Ti	Cr	Other	Al
4.0~4.5	1.2~1.6	0.45~0.7	0.12	0.06	0.25	0.10	0.05	0.15	Remainder

**Table 4.** Mechanical properties of 2524-T3 alloy (source: JIMA Aluminum, n.d.)

Ultimate Tensile Strength, MPa	Yield Strength, MPa	Elongation, %
409~501	359~398	13~15.8

The fuselage skin of contemporary planes is typically made of 2024T3 and 2524-T3 alloys (Tables 1–4) (Aerospace Specification Metals Inc. [ASM], n.d.; JIMA Aluminum, n.d.).

Recently, the aluminum alloy 2024-T3 has been replaced by 2524-T3 due to its greater fracture toughness, which provides better resistance to fatigue crack propagation in panels subjected to tension. With strength and other properties equivalent to those of 2024-T3, fatigue strength has increased by 10% and fracture toughness by 20% compared with 2024-T3 (TM).

Fuselage skin thickness varies from the 0.5 to 2.0 mm (Chatterjee & Bhowmik, 2019). To protect aluminium alloy against corrosion, the sheets of alloys are covered by a layer of aluminum. This cladding doesn't improve strength, but protection against corrosion is still mandatory.

All mentioned sheet materials used for aircraft skin are anisotropic.

### 3. Anisotropy of aluminum alloys sheets for aircraft skin

The process of rolling the alclad alloys sheets leads to the formation of two components of their texture: crystallographic texture, which is caused by the preferred orientations of grains, and mechanical fibering, which is the elongation and alignment of grains. Anisotropy of plastic deformation behavior is almost entirely caused by the preferred orientation of grains (Hosford, 2010).

Crystallographic orientation of metal is described by Miller's indices:  $[hkl]$  represents a direction;  $\langle hkl \rangle$  represents a family of directions;  $(hkl)$  – represents a plane;  $\{hkl\}$  represents a family of planes.

The typical rolling textures in f.c.c. metals and alloys are: copper  $\{112\}\langle 11\bar{1} \rangle$ , Taylor  $\{4\ 4\ 11\}\langle 11\ 11\ \bar{8} \rangle$ , S  $\{123\}\langle 634 \rangle$ , brass  $\{110\}\langle 1\bar{1}2 \rangle$ , and Goss  $\{110\}\langle 001 \rangle$ . Some vari-

ability in the exact indices can be seen, particularly in the S component (Wilkinson, 2001).

For the aluminum layer used for clad layers of our specimens, the preferred orientation after rolling is  $\{112\}\langle 111 \rangle$ , for aluminum alloys, it is  $\{110\}\langle 112 \rangle$  (Wasserman & Greven, 1962).

Crystallographic texture anisotropy can be used to enhance the strength of repaired parts by orienting them for lower resolved shear stresses in the grains of polycrystalline materials.

### 4. Introduction of crystallographic factor into the calculation of equivalent stress

Almost all aircraft parts are subjected to multiaxial loading; at least biaxial in-plane loading in the simplest case of solely pressurization. For stress-strain analysis, the Huber-Mises formula is used. However, the Huber-Mises formula does not take into account the anisotropy of rolled material. Therefore, to achieve the optimal orientation of the anisotropic patch, the crystallographic factor must be introduced into the calculation procedures. The method to do this is described in the work (Maslak & Karuskevich, 2023).

According to the Huber-Mises formula, the equivalent stress can be found as:

$$\sigma = \sqrt{0.5 \left[ (\sigma_x - \sigma_y)^2 + (\sigma_y - \sigma_z)^2 + (\sigma_z - \sigma_x)^2 \right] + \sqrt{3(\tau_{xy}^2 + \tau_{yz}^2 + \tau_{zx}^2)}}, \quad (1)$$

where:  $\sigma_{eq}$  – equivalent Huber-Mises stress;  $\sigma_x$  – longitudinal (axial) stress;  $\sigma_y$  – hoop stress;  $\sigma_z$  – transversal stress;  $\tau_{xy}$ ,  $\tau_{yz}$ ,  $\tau_{zx}$  – shear stress components.

For the combined hoop and longitudinal loading, generated by pressurization and bending considered in this paper, the formula for the Huber-Mises stress is simplified to:

$$\sigma = \sqrt{0.5 \left[ (\sigma_x - \sigma_y)^2 + (\sigma_y)^2 + (-\sigma_x)^2 \right]} \quad (2)$$

The discussed approach arises from numerous studies of the nature of surface deformation relief forming on metals under repeated loads. Direct observation of slip bands on the metal surface has shown that the signs of the relief have a crystallographic nature. Moreover, the transition from uniaxial loading to multiaxial loading leads to the activation of new slip systems (Karuskevych et al., 2012; Pejkowski et al., 2019). Based on these observations, it was decided to consider resolved shear stresses in crystals (Figure 3) (Askeland & Fulay, 2009) instead of stresses calculated without regard to the crystallographic orientation of the grains, and to use these in the Huber-Mises equation.

For biaxial loading by pressurization and bending, the Huber-Mises formula for corrected equivalent stresses gets a view:

$$\sigma_{eq \text{ corrected}} = \sqrt{0.5 \left[ (m\sigma_x - m\sigma_y)^2 + (m\sigma_y)^2 + (-m\sigma_x)^2 \right]} \quad (3)$$

where:  $\sigma_{eq}$  – equivalent Huber-Mises stress corrected to account for crystallographic texture;  $m_i$  – Schmid factor for actuated slip system (Schmid & Boas, 1968). The Schmid factor equals the cosine of the angle with the vector normal to the slip plane ( $\phi$ ) multiplied by the cosine of the angle with the slip direction ( $\lambda$ ).

The correctness of this idea was proved by experiments with aluminium alloys tested under biaxial fatigue loading. A comparison of the two relationships between the number of cycles to failure and equivalent stress, calculated by the conventional Huber-Mises formula (Figure 4a) and the corrected one, is shown below (Figure 4b).

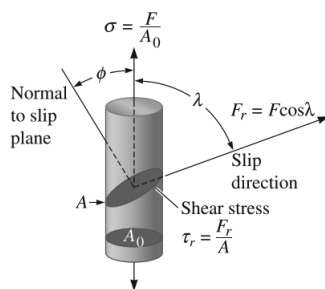


**Figure 3.** Resolved stresses in FCC crystal (source: Askeland & Fulay, 2009)

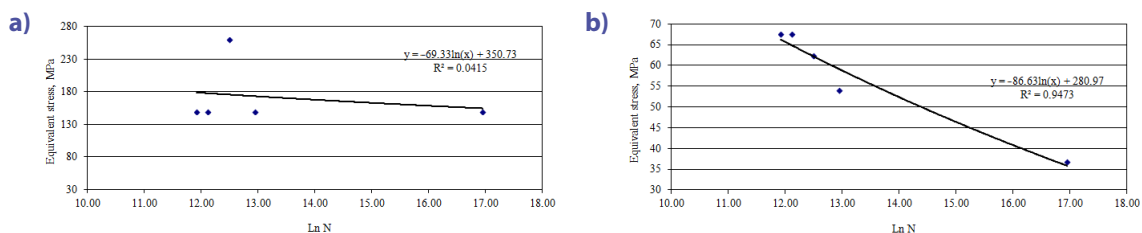


**Figure 4.** Fatigue curves for specimens subjected to biaxial loading: a – conventional Huber-Mises stress; b – corrected Huber-Mises stress

The Figure 4, a depicts the relationship between the number of cycles to failure and the equivalent stress calculated according to the conventional Huber-Mises formula. The correlation is  $R^2 = 0.04$  only. The low correlation value for the conventional Huber-Mises method can be explained by two reasons: a) the Huber-Mises method was proposed for isotropic materials, while industrial sheet materials of aluminium alloys are anisotropic; b) the Huber-Mises method doesn't consider resolved shear stresses on the particular slip systems (slip plane and slip direction) responsible for microplastic deformation during fatigue

The introduction of the crystallographic factor into the Huber-Mises formula increases the correlation between the equivalent stress and the number of cycles to failure from  $R^2 = 0.04$  to 0.94 (Figure 4b).

## 5. Loads on aircraft and stress analysis for aircraft fuselage skin

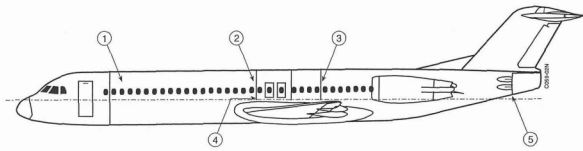
In flight and on the ground, aircraft structure is subjected to loads from turbulence, aerodynamic forces, buffeting, motor vibration, maneuvers, cabin pressurization, airfield unevenness, ground reactions, etc. (European Union Aviation safety Agency, 2023). Almost all these loads are transmitted to and concentrated in the fuselage structure. Loads are transferred via the fuselage structure from one aircraft part to another.

Figure 5 provides a general idea of the loading conditions on a transport aircraft fuselage (Wanhill, 1996).

In general terms, the skin of aircraft fuselages is subjected to the combined loading from cabin pressure, fuselage bending, and twisting, but the distribution of these loads depends on the location of the analyzed zone. The front fuselage withstands pressurization stresses only; the body crown just before the front spar attach frame withstands pressurization and bending stresses; the body crown just behind the rear spar attach frame withstands pressurization and bending stresses; the mid-fuselage before the front spar attach frame is loaded by pressurization and shear stresses; the neutral line area is loaded only by pressurization.

According to Abbishek et al. (2017), fatigue failure accounts for almost 55% of failures. All the mentioned loads fluctuate and contribute to metal fatigue accumulation.

The repair procedure of the fuselage skin by patches or replacement of skin panels must ensure the required



**Figure 5.** Zones of transport aircraft fuselage prone to uniaxial/multiaxial loading conditions: 1 – front fuselage; 2 – body crown just before front spar attach frame; 3 – body crown just behind rear spar attach frame; 4 – mid-fuselage before front spar attach frame; 5 – neutral line (Wanhill, 1996)

level of bearing capacity. This can be achieved by taking into account two important factors: the biaxial stress state of the skin component and the anisotropy of the patch material.

Among the many loading conditions of the fuselage structure, some representative cases were selected to illustrate the necessity and possibility of accounting for crystallographic anisotropy in aircraft repairs by patches.

For the thin-walled structure of the fuselage, hoop stresses from pressurization are considered a primary source of the fatigue damage (A. Skorupa & M. Skorupa, 2012), but the calculations cannot be accepted as completely correct without account for other components of fuselage loading.

Hoop stress in the skin from the pressurization can be found by the equation:

$$\sigma_{hoop} = p \times R/t,$$

where:  $p$  – pressure difference;  $R$  – radius of the skin curvature;  $t$  – skin thickness.

Longitudinal stress from pressurization  $\sigma_n$  equals 0,5  $\sigma_{hoop}$ .

Cabins of contemporary transport category aircraft are pressurized. For the fuselage of a widebody Boeing plane, for example, hoop stress equals 17.4 ksi (120 MPa). Thus, the axial stress is equal to 60 MPa (A. Skorupa & M. Skorupa, 2012).

The yield strength of aluminium alloy 2024T3 is 360 MPa, which means for hoop stress, the margin of safety is 3.0. The stress caused by bending acts together with the longitudinal stress from pressurization (60 MPa), thus to maintain the same margin of safety, the bending stress should also be considered as 60 MPa. These values will be accepted as exemplary input data for the calculation of equivalent stresses below.

For fuselage skin, pressurization is a crucial impact that has caused several disasters at different stages of the aviation era, such as the Comet accidents in 1953 (Withy, 1997) and Boeing 737-200 in 1988 (FAA, 2022). Given the large number of flights, which now typically exceed 80 000 cycles, this factor significantly contributes to accumulated fatigue damage. In addition to pressurization loads, the fuselage is subjected to a wide range of loads, including significant bending in the vertical plane caused mainly by the horizontal stabilizer and elevator action. Under these loads, the upper fuselage skin panels work under

tension while the lower panels are subjected to compression. Torque moments caused by rudder deflection generate a flow of shear stresses. All these stresses should be considered in the multiaxial stress-strain analysis.

Let's consider calculation of equivalent stresses in the repair patch based on the crystallographic nature of the process (Corrected equivalent stress) for some orientations of patches relative to the two stress components caused by pressurization and fuselage bending. The procedure for corrected equivalent stress calculation is described above and in previously published papers (Maslak & Karuskevich, 2023).

The aluminium alloy patch is anisotropic, with the preferred orientation of grains being  $\{110\}\langle 112\rangle$  (Wasserman & Greven, 1962). For this crystallographic orientation, the resolved shear stresses have been found.

The calculation included: assessment of the angles between the axes of loading and directions of slip and slip planes for hoops and longitudinal stresses; assessment of the Schmid factors for all slip systems; calculation of resolved shear stresses for all possible slip systems; calculation of the corrected Huber-Mises stress for selected load cases. Calculations of the angles between the directions of stress components and slip planes and slip directions were made using an online crystallographic calculator (Semiconductor Spectroscopy and Devices, 2020).

## 6. Calculations of corrected equivalent stress for variation of patch orientation

Calculations of corrected equivalent stress has been conducted for two areas of fuselage skin: the first one, where mainly pressurization generates stresses and the second one, where loads from pressurization are combined with bending tension stress.

The first case considers the calculation of corrected equivalent stress from pressurization for patches with texture direction perpendicular to the fuselage axis. The patch is considered to be installed in the front fuselage area and the area close to the neutral line of the fuselage, where pressurization stresses are dominant. Aluminium alloys belong to the Face Centered Cubic (FCC) metals containing four close-packed planes of the form  $\{111\}$  and three close-packed directions of the form  $\langle 110\rangle$  within each plane, giving a total of 12 slip systems (Noh & Yoon, 2024), as shown in Figure 6.

The considered alloys belong to the 2xxx series, with Aluminum, Copper and Magnesium as primary components (Sanders & Marshall, 2023). Resolved shear stresses were found for all 12 slip systems, and the slip systems

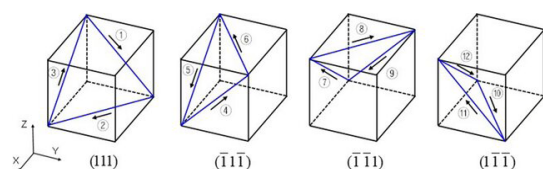


**Figure 6.** Twelve slip systems for FCC metals

**Table 5.** Resolved shear stress caused by the hoop loading for the patch oriented with texture  $\{110\}\langle 112\rangle$  perpendicular the fuselage axis (hoop stress 120 MPa)

Slip plane	Slip direction	The angle between the force direction and the perpendicular to the slip plane, $\lambda$	The angle between the force direction and slip direction, $\psi$	$\text{Cos } \lambda$	$\text{Cos } \psi$	Schmid Factor	Resolved shear component of hoop stress 120 MPa
$(\bar{1}11)$	$[\bar{1}01]$	61.9	106.8	0.47	-0.29	-0.14	16.8
	$[110]$		54.7		0.57	0.27	32.4
	$[011]$		30.0		0.87	0.41	49.2
$(\bar{1}\bar{1}1)$	$[101]$	61.9	30.0	0.47	0.87	0.41	49.2
	$[110]$		54.7		0.57	0.27	32.4
	$[0\bar{1}\bar{1}]$		106.8		-0.29	-0.14	16.8
$(11\bar{1})$	$[\bar{1}10]$	90.0	90.0	0	0	0	0
	$[101]$		30.0		0.87	0	0
	$[011]$		30.0		0.87	0	0
$(111)$	$[\bar{1}10]$	19.5	90.0	-0.94	0	0	0
	$[10\bar{1}]$		106.8		-0.29	0.28	33.6
	$[0\bar{1}\bar{1}]$		106.8		-0.29	0.28	33.6

with maximum resolved shear stresses were selected as the systems responsible for fatigue damage because the dislocations in these systems will begin to move first.

The hoop stress is accepted to be 120 MPa. The longitudinal stress is equal 60 MPa. Results of the resolved shear stresses calculations are shown in Tables 5–7.

The results shown in Table 5 deal with the case when the crystallographic orientation  $\{110\}\langle 112\rangle$  of the patch metal was perpendicular to the longitudinal axis of the fuselage.

The longitudinal component of the fuselage loading acts perpendicular to the direction  $\langle 112\rangle$  of the patch metal; it is parallel to the  $\langle 1\bar{1}\bar{1}\rangle$  indices in the patch metal. This makes it possible to use the crystallographic calculator (Semiconductor Spectroscopy and Devices, 2020) to find the required angles between the loading direction and the slip direction, as well as the angles between the loading direction and the perpendiculars to the slip planes for the assessment of Schmid factors.

**Table 6.** Resolved shear stress caused by longitudinal loading for the patch oriented with texture  $\{110\}\langle 112\rangle$  perpendicular to the fuselage axis (longitudinal stress 60 MPa)

Slip plane	Slip direction	The angle between the force direction and the perpendicular to the slip plane, $\lambda$	The angle between the force direction and slip direction, $\psi$	$\text{Cos } \lambda$	$\text{Cos } \psi$	Schmid Factor	Resolved shear component of longitudinal component 60 MPa
$(\bar{1}11)$	$[\bar{1}01]$	109.5	35.3	-0.33	0.82	0.27	16.2
	$[110]$		35.3		0.82	0.27	16.2
	$[011]$		90.0		0	0	0
$(\bar{1}\bar{1}1)$	$[101]$	109.5	90.0	-0.33	0	0	0
	$[110]$		35.3		0.82	0.27	16.2
	$[0\bar{1}\bar{1}]$		35.3		0.82	0.27	16.2
$(11\bar{1})$	$[\bar{1}10]$	0	90.0	1	0	0	0
	$[101]$		90.0		0	0	0
	$[011]$		90.0		0	0	0
$(111)$	$[\bar{1}10]$	70.5	90.0	0.33	0	0	0
	$[10\bar{1}]$		35.3		0.82	0.27	16.2
	$[0\bar{1}\bar{1}]$		35.3		0.82	0.27	16.2

Accordingly, the angles between the loading direction and the slip directions, and the perpendiculars to the slip planes, are found as the angles between the  $\langle 11\bar{1} \rangle$  vector and the slip directions and the perpendiculars to the slip planes.

Thus, for the patch oriented with texture  $\{110\}\langle 112 \rangle$  perpendicular to the fuselage axis, the resolved shear stresses have two maximum components: from the hoop component of loading, it is equal to 49.2 MPa; from the longitudinal component of loading it is equal 16.2 MPa. Corrected equivalent Huber-Mises stress, calculated by Equation (3) is equal to 43.4 MPa.

In the similar way, a set of cases of stresses from pressurization were considered:

- Resolved shear stress caused by hoop loading from pressurization for the patch oriented with texture  $\{110\}\langle 112 \rangle$  at 45° to the fuselage axis (hoop stress 120 MPa);
- Resolved shear stress caused by longitudinal loading from pressurization for the patch oriented with texture  $\{110\}\langle 112 \rangle$  at 45° to the fuselage axis (longitudinal stress 60 MPa);
- Resolved shear stress caused by hoop loading from pressurization for the patch oriented with texture  $\{110\}\langle 112 \rangle$  along the fuselage axis (hoop stress 120 MPa);
- Resolved shear stress caused by longitudinal loading from pressurization for the patch oriented with texture  $\{110\}\langle 112 \rangle$  along the fuselage axis (longitudinal stress 60 MPa).

Next series of calculations were performed for fuselage crown just before the front spar attach frame and the fuselage crown just behind the rear spar attach frame, subjected to the combined action of pressurization and bending.

Let's consider an example were these stresses equal 60 MPa. Added to the axial stress from pressurization, this results in 120 MPa.

Hoop loads are not influenced by bending; thus, the previously obtained results for hoop stresses can be used for the calculation of stress. No additional hoop stress should be considered for this area of fuselage under the

bending. The resolved shear component of the hoop component (120 MPa) equal 49.2 MPa.

Longitudinal stress combines stress from pressurization and stress from bending, with the total stress equal to 120 MPa.

Additional calculations include:

- Resolved shear stress caused by longitudinal loading and bending for the patch oriented with texture  $\{110\}\langle 112 \rangle$  perpendicular to the fuselage axis (pressurization + bending = 120 MPa);
- Resolved shear stress caused by hoop loading for the patch oriented with texture  $\{110\}\langle 112 \rangle$  at 45° to the fuselage axis (hoop stress = 120 MPa, bending stress = 0);
- Resolved shear stress caused by longitudinal loading and bending for the patch oriented with texture  $\{110\}\langle 112 \rangle$  at 45° to the fuselage axis (hoop stress = 60 MPa plus bending stress = 60 MPa);
- Resolved shear stress caused by hoop loading for the patch oriented with texture  $\{110\}\langle 112 \rangle$  at 90° degrees to the fuselage axis (hoop stress = 120 MPa, bending stress = 0);
- Resolved shear stress caused by longitudinal loading and bending for the patch oriented with texture  $\{110\}\langle 112 \rangle$  at 90° to the fuselage axis (axial stress from pressurization = 60 MPa, bending stress = 60 MPa).

The obtained results make it possible to calculate corrected Huber-Mises stresses for areas of the aircraft structure working under: a) fuselage pressurization conditions; b) combined loading conditions of pressurization and bending (Table 7).

The calculation results shown in Table 7 allow us to draw conclusions about the bearing capacity of the repair patch: it depends on the mutual orientation of the patch's preferred crystallographic orientation (texture) and its loading directions. As the patch operates under multiaxial stress conditions, the analyzing its stress state requires the assessment of equivalent stress.

While the generally accepted method of calculating equivalent stresses according to Huber-Mises does not account for the anisotropy of the sheet materials used

**Table 7.** Results of the equivalent stress calculations according to the conventional and corrected Mises formulas

Pressurization area					
Direction of the patch texture relative to the fuselage axis	Pressurization Hoop stress, MPa	Pressurization Axial stress, MPa	Bending stress, MPa	Mises stress original, MPa	Mises stress corrected, MPa
Perpendicular to the axis	120	60	–	104	43.4
Along the axis	120	60	–	104	29.3
45° to axis	120	60	–	104	49.9
Pressurization plus bending area					
Perpendicular to the axis	120	60	60	120	43.4
Along the axis	120	60	60	120	43.3
45° to axis	120	60	60	120	57.6

in the manufacture and repair of aircraft skin, considering crystallographic anisotropy allows for the installations of the repair patch in a way that maximizes its strength capacity. This is confirmed by the smallest values of the equivalent stresses.

*For the area of the structure that experiences only hoop and axial loads from pressurization*, it is optimal to place the repair patch so that the rolling texture  $\{110\}\langle 112 \rangle$  of the patch aligns with the fuselage axis.

In this case, the equivalent stresses determined by taking into account the dominant crystallographic orientation are 29.3 MPa, while other patches orientations produce equivalent stresses of 43.4 MPa with the patch texture direction perpendicular to the fuselage axis and 49.9 MPa when the patch texture direction is at  $45^\circ$  to the fuselage axis.

*For the zone of the structure loaded by the pressurization and fuselage bending*, installing patches with the texture direction at  $45^\circ$  to the fuselage axis provides a corrected equivalent stress of 576 MPa, whilst patches oriented with the texture perpendicular to the fuselage axis result in 43.4 MPa, and those installed with the texture along the axis also result in 43.4 MPa.

## 7. Conclusions

In-service, aircraft may get damaged by cracks, dents, shootings and corrosion. The structural integrity can be restored by the installation of patches. Integrated into the structure, patches withstand operational loads as bearing components. Both in the air and on the ground, the aircraft structure withstands various forces and moments. As a result of these loads, both structural elements and patches work under multiaxial stress conditions. Under multiaxial loading, the strength of the structures is ensured by stress analysis based on the assessment of equivalent uniaxial stresses. The Huber-Mises rule, used for the assessment of equivalent stresses, doesn't take into account the anisotropy of constructional metals, whereas the sheets of aluminum alloys used for the aircraft skin and patches are anisotropic.

For the first time, it is proposed to consider the anisotropy of patches to increase their bearing capacity under multiaxial cyclical loading.

It is also shown that the accuracy of the Huber-Mises equivalent stress calculations can be improved by application a technique that reflects the crystallographic nature of the fatigue damage processes. This method allows introducing the crystallographic factor into the equation for determining equivalent stresses according to the Huber-Mises concept. To account for the crystallographic aspects of the damage process, the resolved shear stresses in slip systems were considered as components of biaxial loadings.

Introducing the crystallographic factor into the Huber-Mises formula for equivalent stress, as evidenced by the results of the fatigue tests under combined tension and torsion presented in the paper, provides a better correlation between the number of cycles to failure and equivalent

stress than can be obtained using the conventional form of the Huber-Mises formula.

The improvement in the bearing capacity of patches can be achieved by orienting the patches so that the corrected Huber-Mises stresses are minimized.

The correction of the Huber-Mises equation is appropriate when calculating the stress state of structural elements made of materials with a pronounced crystallographic texture.

Further development of the proposed method is aimed at its practical application. It requires consideration of all combinations of possible stress components: hoop and axial stresses from pressurization, as well as stresses from bending and torsion. This analysis should be conducted for all parts of the structure. The obtained data will improve the bearing capacity of repair patches and repair panels.

## Acknowledgements

The authors of the paper highly appreciate the support of the Department of Aircraft Design at the National Aviation University (Kyiv, Ukraine) and the research team of Bydgoszcz University of Science and Technology (Poland).

## Author contributions

M. Karuskevych proposed the idea and methodology of the research and performed data interpretation. S. Ignatovych was responsible for the aircraft loading analysis. T. Maslak carried out the analysis of contemporary alloys' textures and conducted fatigue experiments. O. Karuskevych was responsible for the studying current practices in aircraft repair, equivalent stress calculations and data collection.

## Disclosure statement

Authors declare that they do not have any competing financial, professional, or personal interests from other parties.

## References

- Abbishek, R., Kumar, B. R., & Subramanian, H. S. (2017). Fatigue analysis and design optimization of aircraft's central fuselage. *IOP Conference Series: Materials Science and Engineering*, 225, Article 012031. <https://doi.org/10.1088/1757-899X/225/1/012031>
- Aeronautics guide. (2023). *Forms of aircraft corrosion*. <https://www.aircraftsystemstech.com/2019/04/forms-of-corrosion-aircraft-corrosion.html>
- Askeland, D. R., & Fulay, P. P. (2009). *Essentials of materials science and engineering* (2 ed.). Cengage Learning.
- ASM Aerospace Specification Metals Inc. (n.d.). *Aluminum 2024-T3*. <https://asm.matweb.com/search/SpecificMaterial.asp?bassnum=ma2024t3>
- Aviation. (2015). *How is a fuselage "puncture" repaired?* <https://aviation.stackexchange.com/questions/16761/how-is-a-fuselage-puncture-repaired>

- Chatterjee, B., & Bhowmik, S. (2019). Chapter 9 – Evolution of material selection in commercial aviation industry – a review. In *Sustainable engineering products and manufacturing technologies* (pp. 199–219). Academic Press.  
<https://doi.org/10.1016/B978-0-12-816564-5.00009-8>
- Dauntless aviation. (2009). *What happens when an aircraft is struck by lightning?* <https://www.askacfi.com/914/what-happens-when-aircraft-struck-by-lightning.htm>
- European Union Aviation Safety Agency. (2023). *Easy access rules for large aeroplanes (CS-25) (Amendment 26)*. EASA.  
<https://www.easa.europa.eu/en/downloads/129018/en>
- Federal Aviation Administration. (2023). *Aviation maintenance technician handbook – airframe*. U.S. Department of Transportation Federal Aviation Administration Flight Standards Service.
- Federal Aviation Administration. (2022). *Aloha Airlines Flight 243 (Boeing 737-200)*. [https://www.faa.gov/lessons\\_learned/trans-port\\_airplane/accidents/N73711](https://www.faa.gov/lessons_learned/trans-port_airplane/accidents/N73711)
- FI360 Aero [@fi360aero]. (2020, September 7). *Airbus A320 belly skin panel replacement, Fwd Fuselage, section 13/14* [Image attached] [Post]. X. <https://x.com/fi360aero/status/1303069847396458497/photo/2>
- Hosford, W. F. (2010). *Mechanical behavior of materials*. Cambridge University Press. <https://doi.org/10.1017/CBO9780511810923>
- JIMA Aluminum. (n.d.). *T3 Temper 2524 Aluminum sheet EN AW-2524, plane skin aircraft grade aluminum sheet A2524 AA2524*. <https://www.aluminumalloyplate.com/sale-10379800-t3-temper-2524-aluminum-sheet-en-aw-2524-plane-skin-aircraft-grade-aluminium-sheet-a2524-aa2524.html>
- Karuskevich, M., Karuskevich, O., Maslak, T., & Schepak, S. (2012). Extrusion/intrusion structures as quantitative indicators of accumulated fatigue damage. *International Journal of Fatigue*, 39, 116–121. <https://doi.org/10.1016/j.ijfatigue.2011.02.007>
- Kuznetsov, S., Ozolinsh, E., Ozolinsh, I., Pavelko, I., Pavelko, V., Wevers, & Pfeiffer, H. (June 2007). Lamb wave interaction with a fatigue crack in a thin sheet of Al2024-T3. In *EU Project Meeting on Aircraft Integrated Structural Health Assessment (AISHA)*. Leuven, Belgium.
- Lafiosca, P., Fan, I.-S., Avdelidis, N. P. (2023). *Aircraft skin inspections: Towards a new model for dent evaluation*. ArXiv.  
<https://doi.org/10.1784/insi.2023.65.7.378>
- Maslak, T., & Karuskevich, M. (2023). Introduction of crystallographic factor into the von Mises equivalent stress calculation. *Fatigue & Fracture of Engineering Materials & Structures*, 46(3), 1211–1214. <https://doi.org/10.1111/ffe.13940>
- Noh, D., & Yoon, J. W. (2024). Finite difference based stress integration algorithm for crystal plasticity finite element method. *International Journal of Material Forming*, 17, Article 11. <https://doi.org/10.1007/s12289-023-01806-8>
- Pikryl. (1992). *Pictured is a close-up view of a bullet hole in the fuselage of a US Air Force C-130. The aircraft was fired on while delivering relief supplies to the Somalian village of Belet Huen. A single shot from the ground hit the aircraft. The C-130 was not endangered*. <https://picryl.com/media/pictured-is-a-close-up-view-of-a-bullet-hole-in-the-fuselage-of-a-us-air-force-980a6a>
- Pejkowski, Ł., Karuskevich, M., & Maslak, T. (2019). Extrusion/intrusion structure as a fatigue indicator for uniaxial and multiaxial loading. *Fatigue & Fracture of Engineering Materials & Structures*, 42(10), 2315–2324. <https://doi.org/10.1111/ffe.13066>
- Sanders, R. E., & Marshall, G. J. (2023). *Aluminum: Technology, industry, and applications*. ASM International.  
<https://doi.org/10.31399/asm.tb.atia.9781627084277>
- Schmid, E., & Boas, W. (1968). *Plasticity of crystals with special reference to metals*. F. A. Hughes & Co. Ltd.
- Semiconductor Spectroscopy and Devices. (2020). *Crystallographic calculator*. <https://ssd.phys.strath.ac.uk/resources/crystallography/crystallographic-direction-calculator/>
- Skorupa, A., & Skorupa, M. (2012). *Riveted lap joints in aircraft fuselage: Design, analysis and properties*. Springer Science & Business Media. <https://doi.org/10.1007/978-94-007-4282-6>
- Wanhill, R. J. H. (1996). *Some practical considerations for fatigue and corrosion damage assessment of ageing aircraft* (Report NLR TP 96253 L). ResearchGate.
- Wasserman, G., & Greven, J. (1962). Die verschiedenen Arten von Texturen. In *Texturen metallischer Werkstoffe*. Springer.  
[https://doi.org/10.1007/978-3-662-13128-2\\_2](https://doi.org/10.1007/978-3-662-13128-2_2)
- Wilkinson, A. J. (2001). *Deformation textures, encyclopedia of materials: Science and technology*. Elsevier.  
<https://doi.org/10.1016/B0-08-043152-6/00368-5>
- Withey, P. A. (1997). Fatigue failure of the de Havilland comet I. *Engineering Failure Analysis*, 4(2), 147–154.  
[https://doi.org/10.1016/S1350-6307\(97\)00005-8](https://doi.org/10.1016/S1350-6307(97)00005-8)